Chemistry, Physics and Technology of Surface. 2024. V. 15. N 4. P. 441-455

PACS: 68.08.−p doi: 10.15407/hftp15.04.441

V.M. Gun'ko, V.V. Turov

EFFECTS OF PARTICULATE MORPHOLOGY, TEXTURE, AND SURFACE STRUCTURES OF VARIOUS SORBENTS ON BOUND WATER CHARACTERISTICS AT LOW TEMPERATURES

Chuiko Institute of Surface Chemistry of National Academy of Sciences of Ukraine
17 General Naumov Str., Kyiv, 03164, Ukraine, E-mail: vlad_gunko@ukr.net

The temperature and interfacial behaviors of water bound to various sorbents (silicas, carbons, polymers, etc.) are of interest from both theoretical and practical points of view because a certain amount of water could be always adsorbed from air and can affect the material properties, especially at low temperatures due to possible frost damage. These behaviors could be studied using low-temperature ^{1}H NMR spectroscopy of static samples. The particulate morphology and texture of sorbents were characterized using microscopic and nitrogen adsorption methods. The study well demonstrates the influence of various factors including the morphology, texture, and surface structure of sorbents on the temperature and interfacial behaviors of bound water in the amounts smaller than the pore volume of sorbents. Upon volume infilling of pores by water, the textural and morphological effects (leading to the freezing/melting point depression) could be stronger than the effect of the surface structure (leading to the reorganization of bound water), because only one-two adsorption layers are well sensitive to the surface structure (polar or nonpolar surface functionalities). Therefore, changes in the relative amounts of unfrozen water $C_{uw}(T)/C_{280K}$ vs. temperature (at 200 K < T < 273 K) are similar for very different sorbents such as nanosilica, nano/mesoporous silica gel, and activated carbon (at close water amounts in the hydration range of h = 0.04–0.06 g/g) in contrast to that for microcrystalline cellulose. There are strong effects caused by the bound water amounts that are better observed for sorbents with a great contribution of nanopores, e.g., activated carbon AC–86 possessing very high specific surface area due to significant nanoporosity. A nonmonotonic effect of the amounts of water bound to AC–86 could be explained by nonuniform distribution of O-containing functionalities (mainly located at the edges of carbon sheets at the entrances into slitshaped hydrophobic nanopores). The clustered adsorption of water around these functionalities inhibits penetration of water into nanopores (formed by hydrophobic basal planes) especially at small amounts of water. An increase in the water content causes more intensive diffusion of the water molecules into narrower but less hydrophilic pores of AC–86 that results in enhanced freezing/melting point depression. The obtained results are of interest from a practical point of view since very different and practically important sorbents were analyzed in parallel at low temperatures upon various wetting.

***Keywords**: porous sorbents, disperse sorbents, silica sorbents, carbon sorbents, microcrystalline cellulose, unfrozen water, interfacial phenomena*

INTRODUCTION

The interfacial phenomena related to the temperature behavior and state of bound liquid or gaseous (fluid) compounds depend on many factors including particulate morphology, structure (especially surface polar or nonpolar functionalities), and texture of sorbents, as well as structure, kind, and amounts of sorbates, the presence, content, and type of solutes or co-sorbates, *etc*. [1–11]. To elucidate certain general features and regularities of the interfacial phenomena, one could compare results for different sorbents with the same bound sorbate, *e.g*., water (in the amounts smaller that the pore volume), which is one of the most interesting and unusual sorbates [4, 11–13]. For more comprehensive comparison, sorbents could be composed of nonporous (NPNP, *e.g*., nanosilica, fullerite) and porous (PNP, *e.g*., activated carbon) nanoparticles, carbon nanotubes, porous silica globules (silica gels and ordered mesoporous silicas), polymers (*e.g.*, microcrystalline cellulose, MCC, representing nanofibers), which have very different morphological, structural, and textural characteristics and also characterized by different pore and surface wettability [14–35]. To avoid the effects caused by unbound sorbate fractions, their amounts should be smaller than the pore volume of sorbents.

Low-temperature ^{1}H NMR spectroscopy of static samples is an informative method to study

the temperature and interfacial behaviors and state of sorbed (bound) water and other liquids or gases [4–8, 11]. It allows to separate frozen and unfrozen waters including weakly (WAW) and strongly (SAW) associated waters (due to the difference in the values of the chemical shifts of the proton resonance), weakly (WBW) and strongly (SBW) bound waters (due to the difference in the freezing temperature) compared to bulk water (or unbound water, UBW) [11]. Such a characteristic as the amount of unfrozen water *vs*. temperature could be computed from intensity of the ^{1}H NMR spectra recorded at different temperatures [11] because the used technique allows one to separate unfrozen (mobile) water from frozen (immobile) ice due to a narrow bandwidth (20 kHz) and large difference in the transversion relaxation time for liquid and solid phases.

The aim of this study was to analyze the interfacial phenomena related to water bound to different sorbents (various silicas, activated carbon, multi-walled carbon nanotubes, fullerite $C_{60/70}$, and microcrystalline cellulose) using total and relative contents of unfrozen water as functions of temperature at the degree of hydration (h) smaller than the pore volume of the sorbents. Note that there is no a similar comparative study in the literature. The use of various nanostructured materials allows us to show some general regularities in the temperature and interfacial behavior of water bound alone or with co-adsorbates and solutes to the adsorbents studied, despite the difference in the nature of the materials, organization of their surfaces, particulate morphology, and various porosity.

MATERIALS

Various sorbents: (i) fumed silica (nanosilica) A–300 (Pilot plant of Chuiko Institute of Surface Chemistry (CISC), Kalush, Ukraine) representing a loose powder (Fig. 1 *a*) at low bulk density $\rho_b \approx 0.05$ g/cm^3 [1–3, 11–13, 17, 36]; (ii) mesoporous silica gels Si–40, Si–60 (Fig. 1 *b*), and Si–100 (Merck) [11, 12]; (iii) nano/mesoporous silica gel Gasil 200DF (Crosfield) [37]; (iv) ordered mesoporous silicas MCM–48 and SBA–15 (CISC) [11, 38]; (v) activated carbon (AC) AC–86 at the burn-off degree of 86 % (MAST Carbon International Ltd., UK) [11, 39–44]; (vi) fullerite $C_{60/70}$ (Frantsevich Institute for Problems of Materials Science, Kyiv, Ukraine) representing molecular crystals strongly aggregated [45, 46] (Fig. 1 *e*); (vii) multi-walled carbon nanotubes (MWCNT, CISC) [45, 47] (Fig. 1 *d*); and (viii) microcrystalline cellulose (MCC, Fluka, bulk density of ~ 0.5 g/cm^3, hydration of 0.04 g of water per gram of dry MCC) [11, 29] (Fig. 1 *f*) were studied using low-temperature ^{1}H NMR spectroscopy of static samples [11] with addition of different amounts of bidistilled water. Similar sorbents were described in detail previously [11–13, 17, 29, 36–47].

METHODS

Transmission electron microscopy (TEM) images were recorded using a TECNAI G2 F30 microscope (FEI–Philips, Holland) or JEOL JEM–2100F (Japan) at an operating voltage of 300 kV. A dried sample was added to acetone (chromatographic grade) and sonicated to form uniform suspension. Then a suspension drop was deposited on a copper grid with a thin carbon film. After evaporation of acetone, the particles remained on the film were investigated.

Scanning electron microscopy (SEM) equipment (FE–SEM, Hitachi S–4700, Tokyo, Japan, operating voltage $V = 15$ kV, magnification of ×5000–100000; QuantaTM 3D FEG, FEI, USA, $V = 5$–30 kV; and Zeiss Gemini 300, Carl ZEISS, $V = 0.02$–30 kV) was used to analyze the particulate morphology of sorbents.

The textural characteristics of samples degassed at 453 K for 12 hours were studied using nitrogen adsorption-desorption isotherms (Fig. 2) recorded with Micromeritics ASAP 2420 or ASAP 2405N adsorption analyzers. The specific surface area, SSA (Table 1, S_{BET}) was calculated according to the standard BET method [19]. The total pore volume (Table 1, V_p) was estimated from the nitrogen adsorption at relative pressure $p/p_0 \approx 0.98$–0.99 [20]. The nitrogen adsorption-desorption isotherms were used to compute the pore size distributions (PSD, differential $f_V(R) \sim dV_p/dR$ and $f_S(R) \sim dS/dR$) using molecular density functional theory (DFT) with a self-consistent regularization (SCR) procedure under non-negativity condition and regularization parameter $\alpha = 0.01$. A pore model includes cylindrical (C) pores in silica and voids (V) between spherical silica NPNP packed in random aggregates (CV/SCR method) [39, 44]. For silica gels and ordered mesoporous silicas, the model

includes only cylindrical pores. For carbon and polymer sorbents, the model also includes slitshaped pores (SCV/SCR) (Fig. 3 *d*, Table 1). The differential PSD with respect to the pore volume $f_V(R) \sim dV/dR$, $\int f_V(R)dR \sim V_p$ were recalculated to incremental PSD (IPSD) at $\Phi_V(R_i) = (f_V(R_{i+1}) + f_V(R_i))(R_{i+1} - R_i)/2$ at $\sum\Phi_V(R_i) = V_p$). The $f_V(R)$ and $f_S(R)$ functions were also used to calculate contributions of nanopores (V_{nano} and S_{nano} at $0.35 \text{ nm} < R < 1$ nm), mesopores (V_{meso} and S_{meso} at $1 \text{ nm} < R < 25$ nm), and macropores (V_{macro} and S_{macro} at $25 \text{ nm} < R < 100$ nm) (Table 1) [39, 44]. The non-local DFT [48] (NLDFT, Quantachrome) method was also used to calculate the differential PSD (Fig. 3 *a*–*c*).

Low-temperature ^{1}H NMR spectra of water bound in static samples [11] were recorded using a Varian 400 Mercury spectrometer (magnetic field 9.4 T) utilizing 60–90° pulses of 1–3 μs duration. Each spectrum was recorded by co-addition of eight scans with a 1–3 s delay between each scan. Relative mean errors were less than ± 10 % for signal intensity for overlapped signals, and ± 5 % for single signals. Temperature control was within ± 1 K. To prevent supercooling, the spectra were recorded from T_{min} = 180–210 K for precooled samples heated to T_{max} = 280–290 K at a rate of 5 K/min, steps ΔT = 2–15 K, and maintained for 5 min for data acquisition at each temperature. The T_{min} value (typically corresponding to condition of freezing of practically all bound water) was varied depending on the type of sorbents and it is lower for sorbents with a greater contribution of nanopores (*e.g.*, AC, Si–40, 200DF, and MWCNT). NMR signals of frozen water (ice) and sorbents were not registered for static samples due to a narrow bandwidth (20 kHz) and large difference in transverse relaxation time of mobile and immobile phases [11]. It should be noted that low molecular mobility of sorbates bound in different pores and interacting with various surface sites results in certain broadening of the ^{1}H spectra [11], *i.e.*, this is not consequence of the field nonuniformity in a sample. Additionally, the use of solid-state NMR spectroscopy does not lead to significant narrowing of the spectra of bound sorbates due to the heterogeneity of the systems.

Changes in the Gibbs free energy (ΔG) of bound water (Table 2, ΔG, γ_S) were determined from the temperature dependences of the amounts of unfrozen water (C_{uw} in gram of water per gram of dry sorbent) at T = 180–273 K and tabulated ΔG data for ice [11]. The area under the $\Delta G(C_{uw})$ curve determines interfacial Gibbs free energy, γ_S as the modulus of overall changes in $\Delta G(C_{uw})$ due to interaction of water with a sorbent surface [11]

$$\gamma_S = -A \int_0^{C_{uw}^{max}} \Delta G(C_{uw}) dC_{uw}, \qquad (1)$$

where C_{uw}^{max} is the total amount of unfrozen water at $T = 273.15$ K, and A (> 0) is a constant dependent on the type of units used in this equation.

Unfrozen water bound in pores or at a surface of aggregated NPNP, nanotubes, or cellulose nanocrystals can be in several states such as weakly (WAW) and strongly (SAW) associated waters, weakly (WBW) and strongly (SBW) bound waters. For aqueous suspension of MWCNT (h = 6.67 g/g), a major fraction of water could be assigned to unbound water (UBW) similar to bulk water. The SAW and WAW are differentiated due to different average numbers of the hydrogen bonds per a molecule causing changes in the chemical shift of the proton resonance (δ_H), *e.g.*, δ_H = 4–6 ppm (SAW similar to bulk water) and 0.5–1.5 ppm (WAW) [11]. The SBW and WBW differ in the interaction energy with the surroundings (*e.g.*, changes in the Gibbs free energy $\Delta G < -0.5$ kJ/mol (SBW) or > -0.5 kJ/mol (WBW) and freezing temperature ($T > 265$ K for WBW or $T < 265$ K for SBW) [11]. Water can be frozen in narrower pores at lower temperatures ($T < 273$ K) according to the Gibbs–Thomson relation for the freezing point depression (FPD) for liquids located in cylindrical pores at radius R [4–8, 11]

$$\Delta T_m = T_{m,\infty} - T_m(R) = -\frac{2\sigma_{sl} T_{m,\infty}}{\Delta H_f \rho R} = \frac{k_{GT}}{R}, \qquad (2)$$

where $T_m(R)$ is the melting temperature of ice *vs.* R, $T_{m,\infty}$ the bulk melting temperature, ΔH_f the bulk enthalpy of fusion, ρ the solid density, σ_{sl} the energy of solid-liquid interaction, and k_{GT} is the constant (here 40–90 K nm). Equation (2) was used to determine the cluster size distributions (CSD) ($f_V(R) = dV_{uw}(R)/dR$) of water unfrozen at $T < 273$ K [11] and adsorbed onto solid samples. CSD was converted into incremental CSD (ICSD) $\Phi_V(R_i) = (f_V(R_{i+1}) + f_V(R_i))(R_{i+1} - R_i)/2$ at $\sum\Phi_{V,i}(R)$

= V_{uw}. Integration of the $f_V(R)$ and $f_S(R)$ functions at $R < 1$ nm, $1 \text{ nm} < R < 25$ nm, and $25 \text{ nm} < R < 100$ nm gives the volume and the specific surface area of nano-, meso- and macropores, respectively. The specific surface area (S_{uw}) of adsorbents in contact with bound water (assuming for simplicity that the density of unfrozen bound water $\rho_{uw} = 1$ g/cm^3) can be determined from the amount of this water C_{uw}^{max} (estimating pore volume as $V_{uw} = C_{uw}^{max}/\rho_{uw}$) at $T = 273.15$ K and pore size distribution $f(R)$ with a model of cylindrical pores [11]

$$S_{uw} = \frac{2V_{uw}}{R_{av}} = \frac{2C_{uw}^{max}}{\rho_{uw}} \int_{R_{min}}^{R_{max}} f(R)dR \Big/ \int_{R_{min}}^{R_{max}} f(R)RdR, \quad (3)$$

where R_{min} and R_{max} are the minimal and maximal radii of pores filled by unfrozen water, respectively. In the case of calculations of the structural characteristics of nanopores ($R < 1$ nm), mesopores ($1 \text{ nm} < R < 25$ nm) and macropores ($R > 25$ nm), the R_{min} and R_{max} values are the boundary R values for the corresponding pore types (including $R_{min} = 0.2$ nm for nanopores). The C_{uw}^{max}/ρ_{uw} value should be replaced by the corresponding values of the volumes of nanopores, mesopores, or macropores [11]. The average melting temperature $<T_m>$ was calculated using formula [11]

$$< T_m >= \int_{T_{min}}^{T_0} TC_{uw}(T)dT \Big/ \int_{T_{min}}^{T_0} C_{uw}(T)dT, \quad (4)$$

where $T_0 = 273.15$ K, and T_{min} is the temperature corresponding to $C_{uw} = 0$.

RESULTS AND DISCUSSION

The particulate morphology (Fig. 1) and texture (Table 1, Figs. 2 and 3) of the studied sorbents significantly differ. Some of sorbents are composed of nonporous nanoparticles (NPNP), *e.g.*, A–300 and fullerite, which more strongly aggregated for fullerite than for nanosilica that results in the SSA values different by two orders of magnitude (Table 1, S_{BET}) despite molecular sizes of $C_{60/70}$ are much smaller than that of silica NPNP. Other samples are with porous nanoparticles (AC–86) or nonporous NP (porous silicas) tightly bound in microglobules. MWCNT represent nonuniform carbon nanotubes (Fig. 1 *d*) with a number of defects and residual ash with catalyst nanoparticles because the values of V_{nano}/V_p and S_{nano}/S_{BET} are relatively significant (Table 1) and voids between nanotubes in their aggregates cannot provide such significant contribution of nanopores (Fig. 3 *a*). Only 200DF and AC–86 are predominantly nanoporous with a contribution of narrow mesopores (at $1 \text{ nm} < R < 3$ nm), others are rather mesoporous sorbents (Table 1, S_{meso}, V_{meso}) with certain contributions of nanopores (V_{nano} and S_{nano}) and macropores (S_{macro}, V_{macro}). However, maximum broad PSD are characteristic for A–300 and MWCNT (Fig. 3 *a*, *d*) due to their textural porosity caused by voids between NPNP (A–300) or tubes (MWCNT) in their supra-NP or supra-tube structures. However, there is a significant difference in the porosity of A–300 and MWCNT (Fig. 3 *a*, Table 1) since the former is composed of nonporous nanoparticles (*i.e.*, the porosity is totally textural as voids between NPNP in supra-NP structures), but the latter represents defected nanotubes with nanopores (*i.e.*, the porosity is provided by both voids between nanotubes and nanopores in tube defects). As a whole, nanopores in MWCNT correspond to defects in the tubes or pores in ash particles, but in A–300, nanopores represent narrow voids between adjacent NPNP in their aggregates [49] that gives a small contribution of nanopores (Fig. 3 *a*, Table 1). The MCC powder is composed of loosely packed nanofibers with the textural porosity in the powder at the bulk density of $\rho_b \approx 0.5$ g/cm^3 which corresponds to *ca*. 67 % porosity [50, 51]. It should be noted that the nitrogen adsorption method (Fig. 2) could give the underestimated values of V_{macro} due to the method features caused by very weak interactions of the nitrogen molecules with distant pore walls in macropores [19, 20]. This underestimation could be found not only for fumed silica A–300 but also for MWCNT and MCC due to the particulate morphology and texture of these sorbents (Figs. 1–3).

Additionally, the NLDFT calculations are restricted to the pore radius (half-width) of *ca*. 37.8 nm (Fig. 3 *a–c*) in contrast to SCV/SCR DFT (Fig. 3 *d*). This underestimation effect could be even for AC–86 [11], for which there is no the plateau adsorption of nitrogen at high p/p_0 values (Fig. 2) due to the presence of macropores (invisible within the NLDFT PSD calculations due to the use of the differential PSD in contrast to incremental SCV/SCR DFT PSD, comp.

curves for AC–86 in Fig. 3 *b*, *d*). As a whole, the morphological and textural characteristics of studied sorbents (Figs. 1–3, Table 1) could strongly affect the temperature and interfacial behaviors of bound water located in pores of different sizes (from nano/mesopores to macropores) and shapes (slitshaped and cylindrical pores, voids between NPNP, PNP, nanotubes, nanofibers, *etc*.).

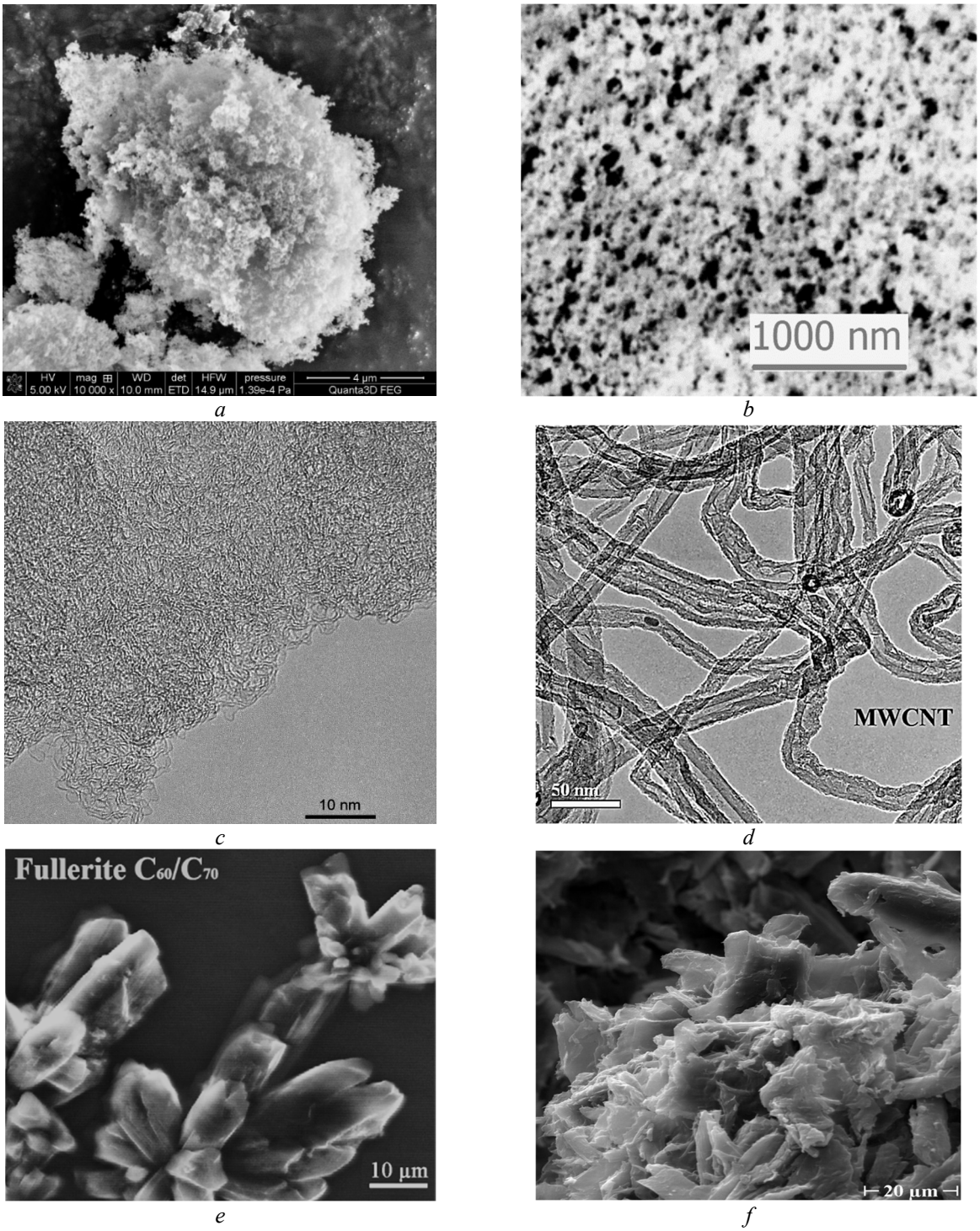

a *b* *c* *d* *e* *f*

Fig. 1. Microscopic images of (*a*) nanosilica A–300 (S_{BET} = 294 m^2/g); (*b*) Si–60; (*c*) AC (S_{BET} = 1664 m^2/g, V_p = 1.486 cm^3/g); (*d*) MWCNT; (*e*) fullerite $C_{60/70}$ [45]; and (*f*) MCC [52] (TEM (*b*-*d*), SEM (*a*, *e*, *f*))

Table 1. Textural characteristics of individual adsorbents (DFT SCV/SCR method)

Material	S_{BET} (m^2/g)	V_p (cm^3/g)	V_{nano} (cm^3/g)	V_{nano}/V_p	V_{meso} (cm^3/g)	V_{macro} (cm^3/g)	S_{nano} (m^2/g)	S_{nano}/S_{BET}	S_{meso} (m^2/g)	S_{macro} (m^2/g)
Si–40	622	0.64	0.077	0.12	0.493	0.066	188	0.30	433	1
Si–60	456	0.82	0.076	0.09	0.746	0	123	0.27	333	0
Si–100	349	1.22	0.011	0.01	1.191	0.022	41	0.12	308	1
200DF	484	0.34	0.244	0.72	0.092	0	429	0.89	55	0
MCM–48	1324	1.17	0.094	0.08	0.956	0.130	340	0.27	975	7
SBA–15	974	1.33	0.058	0.04	1.231	0.045	165	0.17	807	2
A–300	294	0.85	0.023	0.03	0.560	0.266	45	0.15	233	17
MWCNT	346	1.19	0.082	0.07	0.499	0.625	211	0.61	104	31
Fullerite	3	0.012	0	0	0.007	0.005	0.8	0.27	2.1	0.2
AC–86	3463	2.32	1.310	0.56	0.890	0.120	2181	0.63	1279	3

Note. The V_{nano} and S_{nano} values were calculated by integration of the $f_V(R)$ and $f_S(R)$ function, respectively, at 0.35 nm < R < 1 nm, V_{meso} and S_{meso} at 1 nm < R < 25 nm, and V_{macro} and S_{macro} at 25 nm < R < 100 nm

Table 2. Characteristics of unfrozen water bound to different sorbents at various degree of hydration

Sorbent	h (g/g)	C_{uw}^s (mg/g)	C_{uw}^w (mg/g)	$-\Delta G_s$ (kJ/mol)	γ_S (γ_S*) (J/g)	$<T_m>$ (K)	$S_{nano,uw}$ (m^2/g)	$S_{meso,uw}$ (m^2/g)	$V_{nano,uw}$ (cm^3/g)	$V_{meso,uw}$ (cm^3/g)
Si–40	0.576	576	0	3.06	68.4(118.8)	214.4	236	519	0.112	0.464
Si–60	0.766	766	0	2.97	61.8(80.7)	233.7	274	184	0.126	0.640
Si–100	0.376	376	0	2.85	28.9(76.9)	235.7	153	40	0.069	0.307
200DF	0.050	50	0	2.77	6.3(126.0)	211.1	62	18	0.028	0.022
MCM–48	0.200	200	0	2.35	20.8(104.0)	223.0	0	271	0	0.200
SBA–15	0.160	160	0	2.41	17.6(110.0)	220.2	0	232	0	0.160
A–300	0.035	35	0	2.72	4.5(128.6)	212.2	29	3	0.014	0.021
MWCNT	0.071	71	0	3.23	14.3(201.4)	190.0	35	91	0.017	0.054
MWCNT	6.667	120	3850	3.20	21.8(181.7)	264.9	0.1	41	0	0.626
AC–86	0.040	40	0	2.83	5.3(132.5)	207.9	0	52	0	0.040
Fullerite	0.020	20	0	3.09	1.2(60.0)	242.8	0	2	0	0.020
MCC	0.060	27	33	2.63	2.1(77.8)	251.8	18	5	0.007	0.053

Note. ΔG_s is the changes in the Gibbs free energy of the first bound layer of water, $\gamma_S^* = \gamma_S/C_{uw}^s$ (J/g) ($S_{macro,uw} \approx 0$ and $V_{macro,uw} \approx 0$ for all samples with exception of MWCNT suspension at $S_{macro,uw} \approx 30$ m^2/g and $V_{macro,uw} \approx 3.6$ cm^3/g)

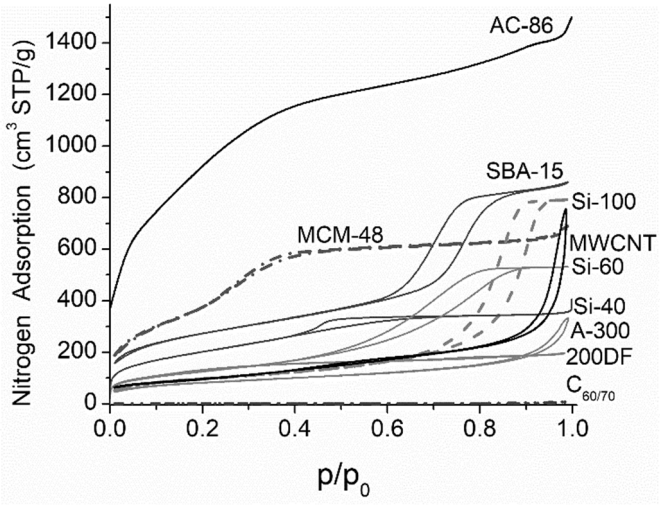

Fig. 2. Nitrogen adsorption-desorption isotherms for studied sorbents

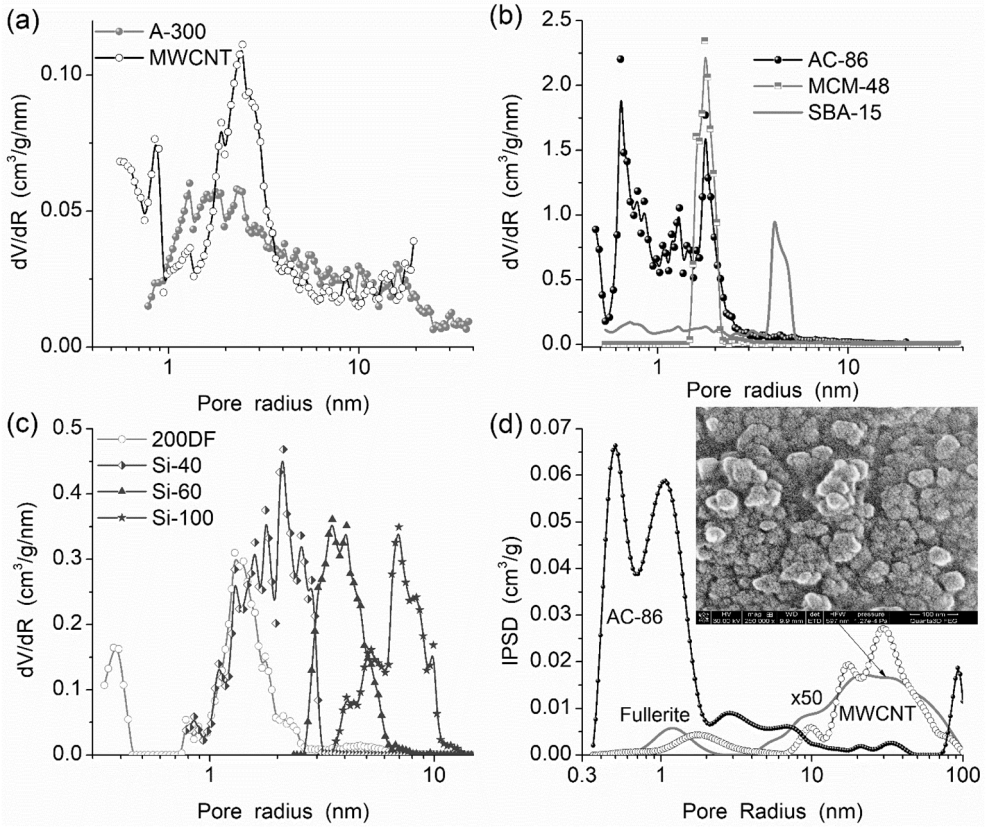

Fig. 3. (*a–c*) NLDFT PSD for various adsorbents: (*a*) nanosilica A–300 and MWCNT, (*b*) activated carbon AC–86 and ordered mesoporous silicas MCM–48 and SBA–15, (*c*) silica gels; and (*d*) incremental SCV/SCR DFT for carbon sorbents: AC-86, MWCNT, and fullerite $C_{60/70}$ (insert: SEM image of fullerite)

The sorbents studied are also characterized by different surface structure and wettability, since carbons (especially in nanopores formed by hydrophobic basal planes) are less hydrophilic than silicas due to different nature of their surfaces and different amounts and surface distributions of polar and nonpolar functionalities at the outer particle surface and pore (void) walls. For example, fullerite $C_{60/70}$ (van-der-Waals molecular crystals, Fig. 1 *e*) does not have any functionality. Therefore, fullerene molecules C_{60} and C_{70} can be tightly bound in molecular crystals strongly aggregated in microglobules (see insert in Fig. 3 *d*). This results in a low value of SSA (since nitrogen or water molecules cannot penetrate into narrow channels between fullerenes in their molecular crystals) corresponding mainly to the outer surface of microglobules. MWCNT (Fig. 1 *d*) could have the functionalities only at defect structures in tubes (or ash particles). Other sorbents have surface hydroxyls (silicas, AC, MCC) or more complex O-containing functionalities (AC, MCC) [1–3, 11–18, 40–43]. This could lead to poor wettability of AC nanopores (formed by hydrophobic planar basal sheets) because O-containing functionalities could be located in mesopores at the entrances into nanopores [11, 40–43]. Therefore, water, which tends to the clustered sorption [11], could be located mainly in mesopores of carbon sorbents and may block the entrances into the hydrophobic nanopores.

As a whole, the availability of a set of morphological, textural, and structural factors makes difficult direct comparison of the $C_{uw}(T)$ functions for water (of different amounts) bound to different sorbents studied (Fig. 4). However, there is a certain regularity. If the h value is much smaller than the pore volume (especially nanopore volume, Table 1, V_{nano}) that the greater the contribution of nanopores (Table 1, V_{nano}/V_p and S_{nano}/S_{BET}) the stronger is the displacement of the plateau value (all water is unfrozen) of C_{uw} toward lower temperatures (Fig. 4) (all water is SBW and $C_{uw}^s = h$); *e.g.*, the curve course differences are observed for A–300, MCC,

200DF, and AC–86. However, this effect is much better observed for the normalized $C_{uw}(T)/C_{280K}$ functions (Fig. 5).

The used amounts of water (Figs. 4 and 5, h values) are typically smaller than the pore volume (Table 1, V_p). Therefore, water can be predominantly located in nanopores and mesopores. Therefore, it represents only SBW, which could be unfrozen at $T < 265$ K. This leads to the appearance of a plateau of the $C_{uw}(T)$ (Fig. 4) and $C_{uw}(T)/C_{280K}$ (Fig. 5) functions (at $T < 273$ K) that could be observed in different temperature ranges depending on the morphological and textural characteristics of sorbents.

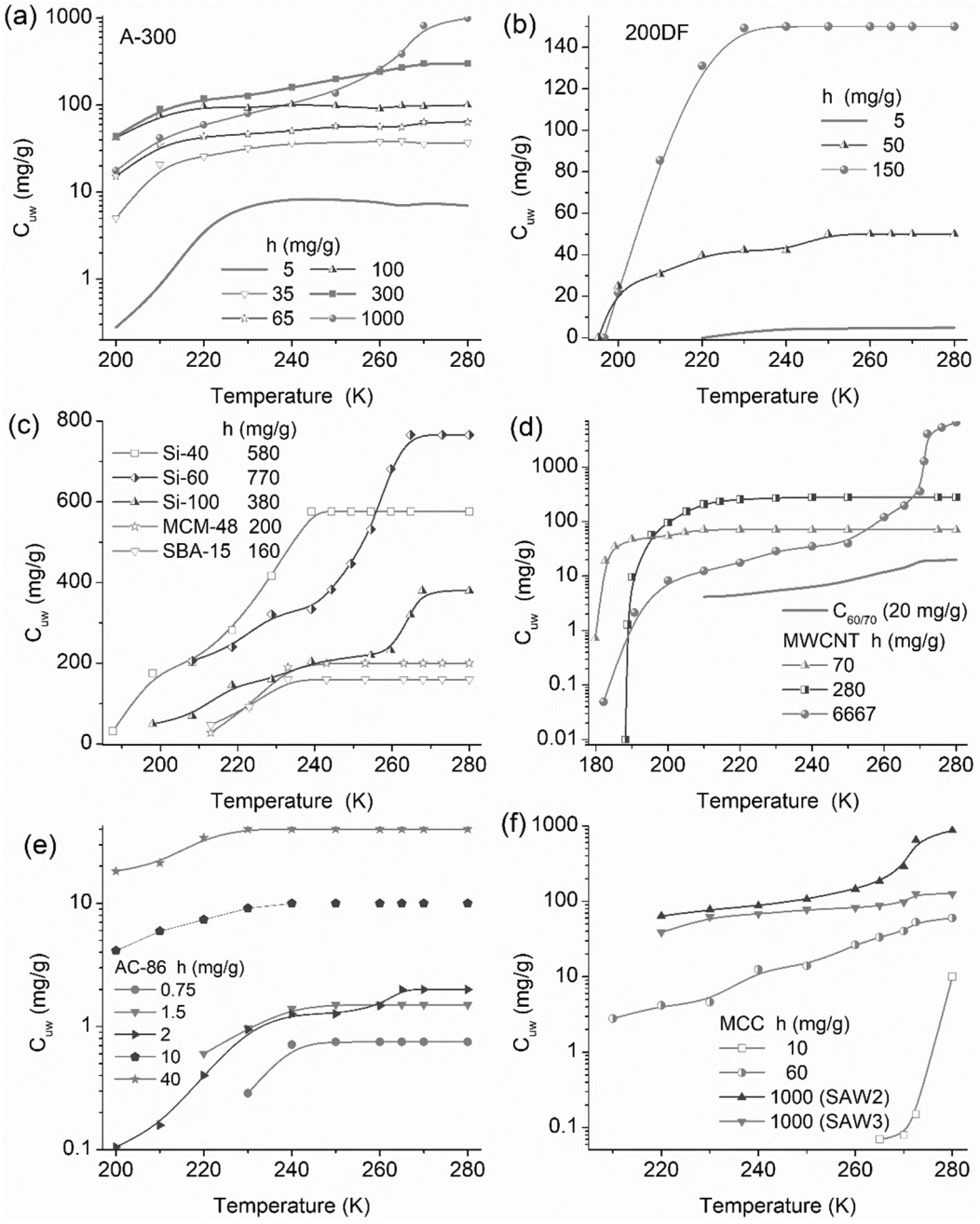

Fig. 4. Amounts of unfrozen water *vs*. temperature at different degree of hydration (h) for: (*a*) fumed silica A–300, (*b*) silica gel 200DF, (*c*) silica gels and ordered mesoporous silicas, (*d*) fullerite $C_{60/70}$ and MWCNT, (*e*) activated carbon AC–86, and (*f*) MCC (with split SAW lines)

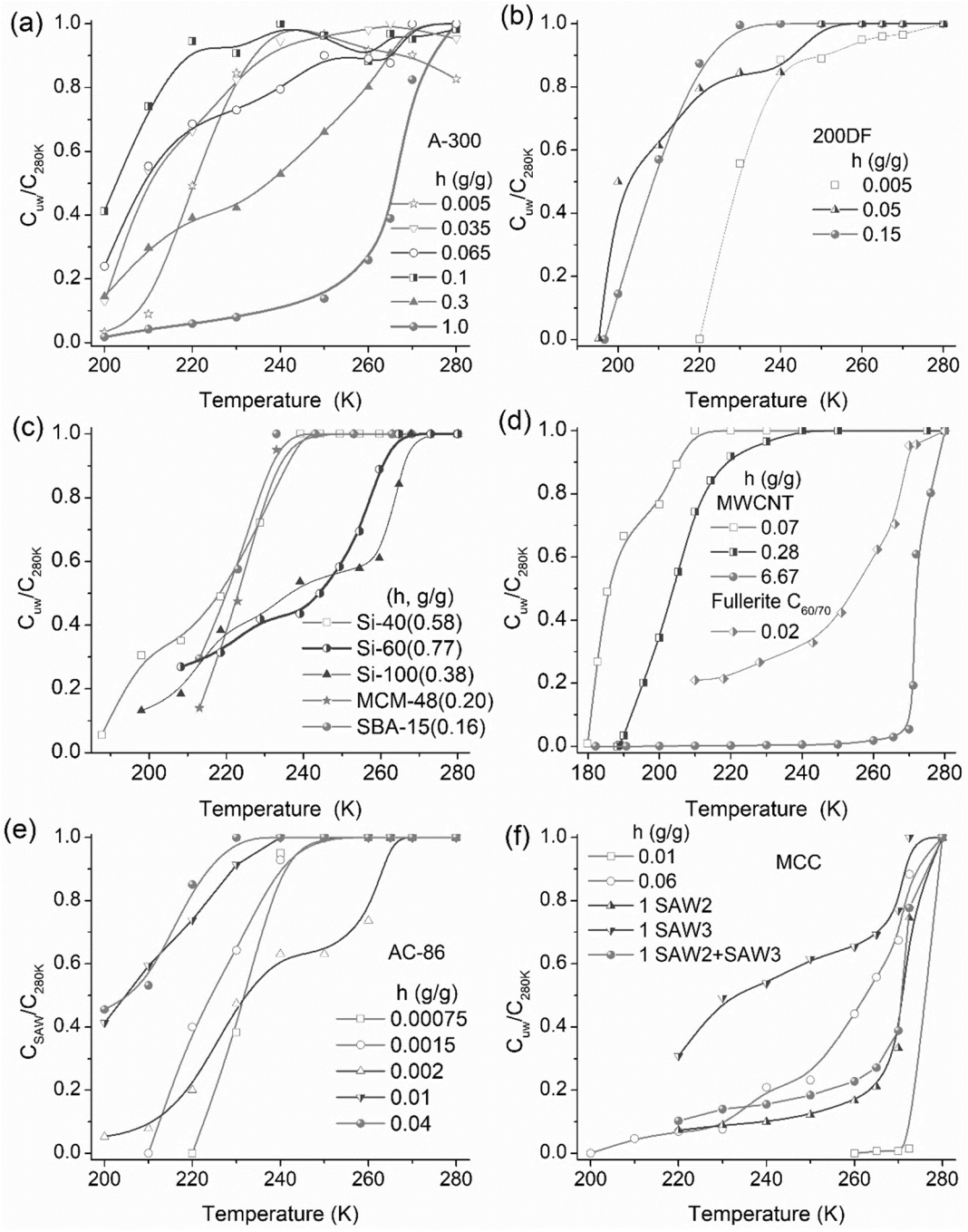

Fig. 5. Relative content of unfrozen water *vs*. temperature at different degree of hydration for: (*a*) fumed silica A–300, (*b*) silica gel 200DF, (*c*) silica gels and ordered mesoporous silicas, (*d*) fullerite and MWCNT, (*e*) activated carbon, and (*f*) MCC

However, the plateau in the $C_{uw}(T)$ functions is absent for A–300 at $h > 0.1$ g/g, MCC, and fullerite (Fig. 4), which are composed of nonporous NP or nanofibers. For porous silicas (Fig. 4 *b*, *c*), MWCNT (Fig. 4 *d*), and AC–86 (Fig. 4 *e*), the $C_{uw}(T)$ plateau is observed but at a different start point due to the difference in the pore sizes of these sorbents (Fig. 3). For a simpler and more clear analysis, one could use the relative content of unfrozen water $C_{uw}(T)/C_{280K}$ normalized to the total amounts of water registered in the ^{1}H NMR spectra at 280 K (Fig. 5). These curves clearly show the absence of the plateau for A–300 (Fig. 5 *a*). For 200DF (Fig. 5 *b*), there is no the plateau at a minimal *h* value because of poor wettability of narrow pores

upon interaction with a small amount of water. For porous silicas (Fig. 5 *c*), a significant displacement of the plateau toward higher temperatures is observed for Si–60 and Si–100 which possess broader pores than Si–40 and 200DF (Fig. 3 *c*). For MWCNT (Fig. 5 *d*), an increase in the water amount leads to the same effect. A more complex behavior of bound water is observed for AC–86 (Fig. 5 *e*) demonstrating the mentioned effect at lower amounts of water (h = 0.00075–0.002 g/g), but at higher amounts of water (h = 0.01 and 0.04 g/g), there is the opposite effect with the displacement of the plateau toward lower temperatures. This could be explained by better penetration of water into narrower pores at its greater amounts that results in stronger freezing/melting point depression in narrower pores. It should be noted that the FPD is stronger for MWCNT (h = 0.071 g/g) than for AC–86 (h = 0.04 g/g) since $<T_{m,MWCNT}> < <T_{m,AC-86}>$ and γ_S/C_{uw} is larger for MWCNT than AC–86 (Table 2) that is rather unexpected result. It is caused by both textural and structural features of these carbons. For MCC (Fig. 5 *f*), the plateau is absent for any amount of bound water, the γ_S* is low, but $<T_m>$ is relatively high (Table 2) due to the morphology and texture of MCC composed of nonporous nanofibers. Similar results are for practically nonporous and hydrophobic fullerite (Table 2) that possesses mesopores and macropores (Figs. 2 and 3, Tables 1 and 2) only as voids in supra-NP structures. For different sorbents containing similar amounts of bound water (h = 0.04–0.06 g/g), the $C_{uw}(T)/C_{280K}$ curves could be similar with exception of MCC (Fig. 6), which characterized by maximal $<T_m>$ value (Table 2) due to a weak FPD effect. This could be explained by features of the particulate morphology and texture of MCC (see inserts with microscopic images in Fig. 6) and other sorbents (Figs. 1–7, Tables 1 and 2).

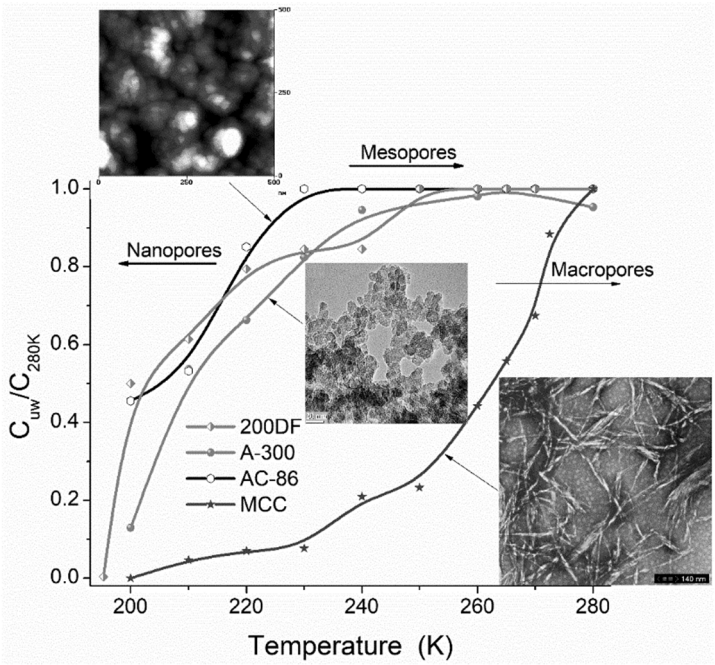

Fig. 6. Relative content of unfrozen water *vs*. temperature at similar low degree of hydration (h = 0.04–0.06 g/g) for selected adsorbents

The size distributions of pores infilled by unfrozen water (Fig. 7) give a clear picture on location of unfrozen water bound in pores of different sizes of sorbents *per se* and in secondary pores formed between the pore walls of sorbents and ice clusters located in pores. Note that the ^{1}H NMR spectra were recorded upon heating from T_{min} toward T_{max} and ice located in narrower pores is melt at lower temperatures. The effect of the secondary porosity is clearly visible from comparison of the NLDFT PSD (Fig. 3) and PSD_{uw} (Fig. 7). For example, for SBA–15 and MCM–48 (Fig. 7 *b*), PSD_{uw} correspond to pores of sizes smaller than that observed in the NLDFT

PSD (Fig. 3). Similar effects are observed for other sorbents since they possess relatively broad PSD and frozen water (ice) clusters could be located in mesopores and macropores that provide the secondary porosity for unfrozen water fraction. Note that the FPD effect could be stronger for the first water layer located at a surface of sorbents [11]; therefore, not all ice is melting in a mesopore at a certain temperature and liquid water layer could appear at pore wall surface before melting residual ice. For silica gels, contributions of nanopores with unfrozen water (Table 2, $S_{nano,uw}$ and $V_{nano,uw}$) are larger than the related values determined from the nitrogen adsorption (Table 1, S_{nano} and V_{nano}). Similar results are observed for other adsorbents (Figs. 3 and 7, Tables 1 and 2). However, the absolute values of S_{uw} and V_{uw} (Table 2) could be lower than the related values estimated from the nitrogen adsorption data (Table 1) because bound water amounts are typically smaller than the pore volume (V_p).

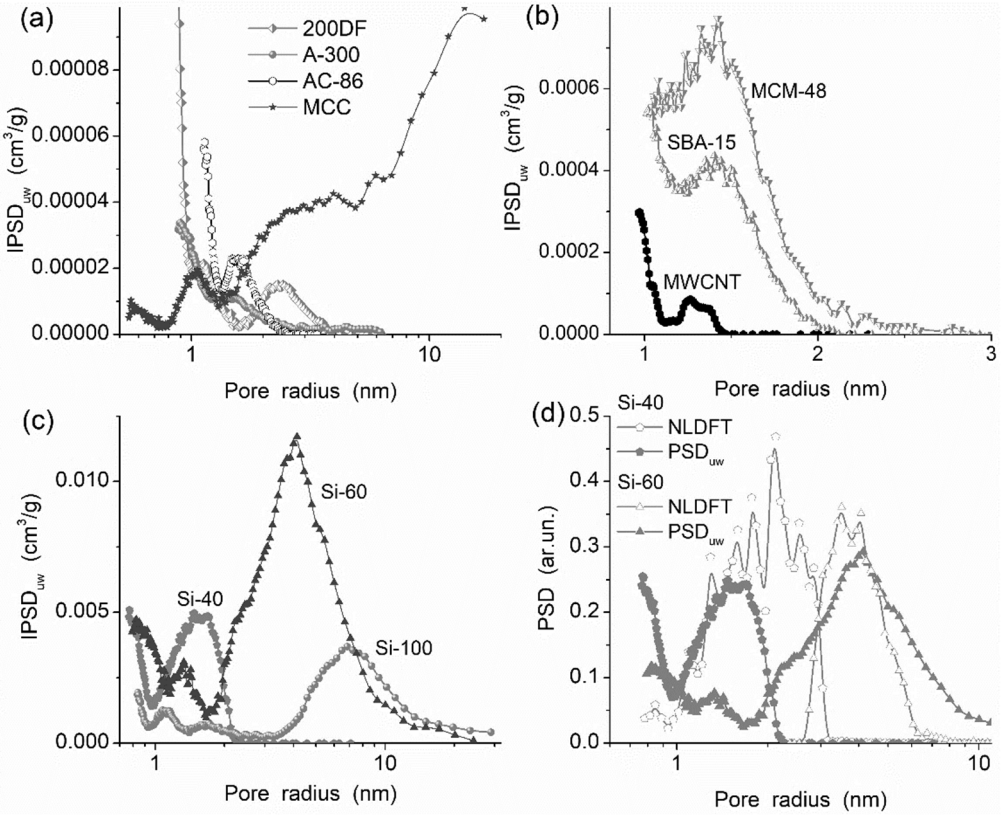

Fig. 7. (*a–c*) Incremental PSD_{uw} related to pores infilled by unfrozen water for various adsorbents, and (*d*) comparison of PSD_{uw} and NLDFT for silica gels

WBW (Table 2, C_{uw}^{w}) is observed in concentrated aqueous suspension of MWCNT (h = 6.67 g/g) and for weakly wetted MCC (h = 0.06 g/g), despite the presence of nanopores in both sorbents (Table 2, $S_{nano,uw}$, $V_{nano,uw}$). AC–86 and SBA–15 possess nanopores with significant and minor contributions, respectively (Fig. 3, Table 1). However, water is not bound in nanopores of AC–86 and SBA–15 (Table 2, $S_{nano,uw}$ = 0 and $V_{nano,uw}$ = 0). This result could be explained by the hydrophobicity of nanopores of both sorbents. For SBA–15, the surface of nanopores is composed of the siloxane bridges, which are not strongly hydrophilic [1–3]. Therefore, the $|\Delta G_s|$ values (Table 2) are relatively small for both AC–86 and SBA–15. However, the average melting temperature $<T_m>$ is relatively low that can be explained by location of bound water in narrow mesopores (Fig. 7). The maximal value of $|\Delta G_s|$ is observed for MWCNT that could be considered as rather unusual result. This could be explained by the presence of O-containing functionalities in nanoporous (plus narrow mesopores) defects in nanotubes, the presence of a certain amount of ash (carbon nanoparticles with catalyst nanoparticles of metal

oxides). However, the amounts of water bound (SBW+WBW) to MWCNT are relatively small for both wetted and suspended samples because the γ_S values (Table 2) are not maximal and unfrozen water is located mainly in narrow mesopores (Fig. 7). The maximal γ_S values are observed for more strongly wetted mesoporous Si–40 and Si–60 containing only SBW and relatively high $|\Delta G_s|$ values. Unfrozen water is mainly located in mesopores (Fig. 7 *c*, Table 2, $V_{meso,uw}$). However, a certain fraction of bound water is located in nanopores ($V_{nano,uw}$, $S_{nano,uw}$) that could be explain by the formation of the secondary porosity as voids between the silica pore walls and ice clusters located in these mesopores. Thus, the temperature and interfacial behaviors of water bound to different sorbents are complex due to a set of factors affecting the related phenomena.

CONCLUSION

The interfacial behavior of water bound to various silicas (fumed silica, silica gels, ordered mesoporous silicas), carbons (activated carbon, multi-walled carbon nanotubes, fullerite), and microcrystalline cellulose demonstrates strong influence of a number of factors including the morphology, texture, and surface structure of sorbents as well as the water amounts and temperature. The textural and morphological effects, *e.g.*, freezing/melting point depression, could be stronger than the effect of the surface structure affecting the water layer organization. For example, the $C_{uw}(T)/C_{280K}$ functions at close water amounts in the range of h = 0.04–0.06 g/g (water is located only in nanopores and narrow mesopores) are similar for nanosilica A–300, nano/mesoporous silica gel 200DF, and activated AC–86 (having different surface structure) in contrast to that for microcrystalline cellulose characterized only by textural porosity as voids between nonporous nanofibers without narrow pores. Especially strong and unusual effects of the water amounts are observed for sorbents with a large contribution of nanopores, *e.g.*, AC–86 with very high specific surface area. The nonmonotonic effect of the content of water bound to AC–86 (*e.g.*, the position and temperature range of the $C_{uw}(T)$ plateau) is due to nonuniform distribution of O-containing functionalities, mainly located at the edges of carbon sheets in mesopores at the entrances into less hydrophilic slitshaped nanopores. The clustered adsorption of water around these functionalities inhibits penetration of water into nanopores especially at small amounts of water. An increase in the water amounts causes more intensive diffusion of the water molecules into narrower but more hydrophobic nanopores that results in the enhanced freezing/melting point depression, which more strongly depends on the pore size than the structure of the pore walls. The obtained results are of interest from a practical point of view since very different and practically important sorbents are studied in parallel. The applications of the studied materials as oral sorbents, drug delivery, industrial adsorbents and filles, etc., which are being in aqueous media or can adsorb water from air; water practically always affects the properties and characteristics of the materials, deal with the effects of interfacial water. The studied interfacial and temperature behaviors of bound water show that the properties of bound water or solutions strongly differ from those of bulk water. Therefore, these effects should be considered in detail upon the practical applications of various adsorbents.

ACKNOWLEDGEMENTS

The authors are grateful to Dr. I. Protsak (University of Vienna) and Dr. hab. B. Charmas (MCSU, Lublin) for some experimental data.

Вплив морфології частинок, текстури та будови поверхні різних сорбентів на характеристики зв'язаної води при низьких температурах

В.М. Гунько, В.В. Туров

Інститут хімії поверхні ім. О.О. Чуйка Національної академії наук України
вул. Генерала Наумова, 17, Київ, 03164, Україна, vlad_gunko@ukr.net

Температурна та межфазна поведінка води, зв'язаної з різними сорбентами (кремнеземом, вуглецем, полімерами тощо), являє інтерес як з теоретичної, так і з практичної точок зору, оскільки певна кількість води може адсорбуватися з повітря та може впливати на властивості матеріалу, особливо при низьких температурах через можливе пошкодження при заморожуванні води. Цю поведінку можна вивчити за допомогою низькотемпературної ^{1}H ЯМР-спектроскопії статичних зразків. Морфологію та структуру частинок досліджуваних сорбентів охарактеризовано за допомогою мікроскопічних та азотно-адсорбційних методів. Дослідження добре демонструє вплив різних факторів, включаючи морфологію, текстуру та структуру поверхні сорбентів, на температурну та межфазну поведінку зв'язаної води в кількостях, менших за об'єм пор сорбентів. При об'ємному заповненні пор водою текстурні та морфологічні ефекти (що призводять, наприклад, до зниження точки замерзання/плавлення) можуть бути сильнішими, ніж вплив структури поверхні (що призводить, наприклад, до реорганізації зв'язаної води), оскільки лише один-два адсорбційних шари добре чутливі до структури поверхні (тобто полярних чи неполярних поверхневих структур). Таким чином, відносні кількості незамерзлої води $C_{uw}(T)/C_{280K}$ (при 200 K < T < 273 K) подібні для дуже різних сорбентів, таких як нанокремнезем А–300, нано/мезопористий силікагель 200DF та активований вуглець АС–86 (при близькій кількості води в інтервалі гідратації h = 0.04–0.06 г/г) на відміну від мікрокристалічної целюлози. Існують сильні ефекти, викликані різною кількістю води, які краще спостерігаються для сорбентів із великим вмістом нанопор, наприклад, АС–86, що має дуже високу питому поверхню через значну нанопористість. Немонотонний ефект кількості води, зв'язаної з АС–86, можна пояснити нерівномірним розподілом О-вмісних функціональних груп (переважно розташованих на краях вуглецевих листів на входах у щілиноподібні гідрофобні нанопори). Кластерна адсорбція води навколо цих функціональних структур перешкоджає проникненню води в нанопори (утворені гідрофобними базальними площинами), особливо при невеликих кількостях води. Збільшення вмісту води викликає більш інтенсивну дифузію молекул води у вужчі пори але менш гідрофільні, що призводить до посиленого зниження точки замерзання/плавлення. Отримані результати являють інтерес з практичної точки зору, оскільки паралельно аналізувалися дуже різні та практично важливі сорбенти.

***Ключові слова**: пористі сорбенти, дисперсні сорбенти, кремнеземні сорбенти, вуглецеві сорбенти, мікрокристалічна целюлоза, рідка вода, явища на межах поділу*

REFERENCES

1. Iler R.K. *The Chemistry of Silica. Solubility, Polymerization, Colloid and Surface Properties, and Biochemistry*. (Chichester: Wiley, 1979).
2. Bergna H.E., Roberts W.O. *Colloidal Silica: Fundamentals and Applications*. (Boca Raton: CRC Press, 2006).
3. Somasundaran P. *Encyclopedia of Surface and Colloid Science*. Third Edition. (Boca Raton: CRC Press, 2015).
4. Chaplin M. *Water structure and science*. http://www1.lsbu.ac.uk/water/, accessed on 2 October, 2023.
5. Kimmich R. *NMR Tomography, Diffusometry, Relaxometry*. (Heidelberg: Springer, 1997).
6. Petrov O.V., Furó I. NMR cryoporometry: Principles, applications and potential. *Prog. Nucl. Magn. Reson. Spectrosc.* 2009. **54**(2): 97.
7. Mitchell J., Webber J.B.W., Strange J.H. Nuclear magnetic resonance cryoporometry. *Phys. Rep*. 2008. **461**(1): 1.
8. Strange J.H., Rahman M., Smith E.G. Characterization of porous solids by NMR. *Phys. Rev. Lett*. 1993. **71**(21): 3589.
9. Babick F. *Suspensions of Colloidal Particles and Aggregates*. (Berlin: Springer, 2018).
10. Koduru J.R., Karri R.R., Mubarak N.M., Bandala E.R. *Sustainable Nanotechnology for Environmental Remediation*. (Amsterdam: Elsevier, 2022).
11. Gun'ko V.M., Turov V.V. *Nuclear Magnetic Resonance Studies of Interfacial Phenomena*. (Boca Raton: CRC Press, 2013).

12. Gun'ko V.M., Turov V.V., Zarko V.I., Goncharuk E.V., Gerashchenko I.I., Turova A.A., Mironyuk I.F., Leboda R., Skubiszewska-Zięba J., Janusz W. Comparative characterization of polymethylsiloxane hydrogel and silylated fumed silica and silica gel. *J. Colloid Interface Sci*. 2007. **308**(1): 142.
13. Gun'ko V.M., Turov V.V., Goncharuk O.V., Pakhlov E.M., Matkovsky O.K. Interfacial phenomena at a surface of individual and complex fumed nanooxides. *Surface*. 2019. **11(26)**: 3.
14. *Ullmann's Encyclopedia of Industrial Chemistry*. *Cryogenic Technology.* (Weinheim: Wiley–VCH, 2007).
15. *Kirk–Othmer Encyclopedia of Chemical Technology*. V. 1, 13, 22, and 26. (John Wiley & Sons, Inc. 2001).
16. Bhushan B. *Encyclopedia of Nanotechnology*. (Dordrecht: Springer, 2012). P. 3917.
17. *Basic characteristics of Aerosil fumed silica.* (4th ed.) Tech. Bull. Fine Particles 11. (Hanau: Evonik Industries, 2014).
18. Legrand A.P. *The Surface Properties of Silicas*. (New York: Wiley, 1998).
19. Adamson A.W., Gast A.P. *Physical Chemistry of Surface*. 6th edition. (New York: Wiley, 1997).
20. Gregg S.J., Sing K.S.W. *Adsorption, Surface Area and Porosity*. 2nd ed. (London: Academic Press, 1982).
21. Kulkarni P., Baron P.A., Willeke K. *Aerosol Measurement: Principles, Techniques, and Applications*. Third Edition. (New York: John Wiley & Sons, 2011).
22. Büchel K.H., Moretto H.-H., Woditsch P. *Industrial Inorganic Chemistry*. (Weinheim: Wiley-VCH, 2000).
23. Xu R., Yan Xu Y. *Modern Inorganic Synthetic Chemistry*. (Elsevier: Amsterdam, 2017).
24. Radoor S., Karayil J., Jayakumar A., Kandel D.R., Kim J.T., Siengchin S., Lee J. Recent advances in cellulose- and alginate-based hydrogels for water and wastewater treatment: A review. *Carbohydr. Polym*. 2024. **323**: 121339.
25. Cousins S.K., Brown M.B. Cellulose in microfibril assembly: computational molecular mechanics energy analysis favours bonding by Van der Waals forces as the initial step in crystallization. *Polymer.* 1995. **36**(20): 3885.
26. Hatakeyama H., Hatakeyama T. Interaction between water and hydrophobic polymers. *Termochem. Acta*. 1998. **308**(1–2): 3.
27. Hatakeyama T., Nakamura K., Hatakeyama H. Determination of bound water content in polymers by DTA, DSC and TG. *Termochem. Acta*. 1988. **123**: 153.
28. Heiner A.P., Teleman O. Interaction between monoclinic crystalline cellulose and water: breakdown of the odd/even duplicity. *Langmuir.* 1997. **13**(3): 513.
29. Turov V.V., Gun'ko V.M., Barvinchenko V.N., Rugal A.A., Turova A.A., Fedyanina V.V. Hydration of cellulose with the presence of quercetin and organic solvents. *Chemistry, Physics, and Technology of Surface*. 2009. **15**: 169.
30. Ahuja S. (Editor). *Separation Science and Technology*. V. 15. (Amsterdam: Elsevier, 2022).
31. Ngu L.H. *Carbon Capture Technologies*. (Amsterdam: Elsevier, 2022).
32. Yang R.T. *Adsorbents: Fundamentals and Applications*. (New York: Wiley, 2003).
33. Lu K. *Nanoparticulate Materials. Synthesis, Characterization, and Processing.* (Hoboken, New Jersey: John Wiley & Sons, Inc., 2013).
34. Moreno-Piraján J.C., Giraldo-Gutierrez L., Gómez-Granados F. *Porous Materials Theory and Its Application for Environmental Remediation*. (Cham: Springer Nature, 2021).
35. Rousseau R.W. *Handbook of Separation Process Technology*. (New York: John Wiley & Sons, 1987).
36. Gun'ko V.M., Turov V.V., Pakhlov E.M., Krupska T.V., Charmas B. Effect of water content on the characteristics of hydro–compacted nanosilica. *Appl. Surf. Sci*. 2018. **459**: 171.
37. Blitz I.P., Blitz J.P., Gun'ko V.M., Sheeran D.J. Functionalized silicas: structural characteristics and adsorption of Cu(II) and Pb(II). *Colloids Surf. A*. 2007. **307**(1–3): 83.
38. Gun'ko V.M., Turov V.V., Turov A.V., Zarko V.I., Gerda V.I., Yanishpolskii V.V., Berezovska I.S., Tertykh V.A. Behaviour of pure water and water mixture with benzene or chloroform adsorbed onto ordered mesoporous silicas. *Cent. Eur. J. Chem*. 2007. **5**: 420.
39. Gun'ko V.M. Morphological and textural features of various materials composed of porous or nonporous nanoparticles differently packed in secondary structures. *Appl. Surf. Sci.* 2021. **569**: 151117.
40. Bansal R.C., Donnet J.B., Stoeckli F. *Active Carbon*. (New York: Marcel Dekker, 1988).
41. McEnaney B., Mays T.J., Rodriguez-Reinoso F. (editors). Fundamental Aspects of Active Carbons. Special issue. *Carbon*. 1998. **36**(10).
42. Cooney D.O. *Activated Charcoal in Medical Applications*. (New York: Marcel Dekker, 1995).
43. Rodriguez-Reinoso F., McEnaney B., Rouquerol J., Unger K. (editors). *Studies in Surface Science and Catalysis.* V. 144. *Characterisation of Porous Solids VI*. (Amsterdam: Elsevier Science, 2002).
44. Gun'ko V.M. Features of the morphology and texture of silica and carbon adsorbents. *Surface*. 2021. **13(28)**: 127.

45. Gun'ko V.M., Turov V.V., Schur D.V., Zarko V.I., Prykhod'ko G.P., Krupska T.V., Golovan A.P., Skubiszewska-Zięba J., Charmas B., Kartel M.T. Unusual interfacial phenomena at a surface of fullerite and carbon nanotubes. *Chem. Phys*. 2015. **459**: 172.
46. Kroto H.W., Fischer J.E., Cox D.E. (editors). *The Fullerenes*. (Oxford: Pergamon Press, 1993).
47. Harris P.J.F. *Carbon Nanotube Science. Synthesis, Properties and Applications*. (Cambridge: Cambridge University Press, 2009).
48. Ravikovitch P.I., Neimark A.V. Density functional theory model of adsorption on amorphous and microporous silica materials. *Langmuir.* 2006. **22**(26): 11171.
49. Hashim A.A. *Smart Nanoparticles Technology*. (Rijeka, Croatia: InTech, 2012).
50. Rahman M.R. (editor). *Fundamentals and Recent Advances in Nanocomposites Based on Polymers and Nanocellulose*. (Elsevier, 2021).
51. Barhoum A., Bechelany M., Makhlouf A.S.H. (editors). *Handbook of Nanofibers*. (Springer, 2019).
52. Universität Bayreuth. Laboratory for Soft Matter Electron Microscopy. https://www.smem.uni-bayreuth.de/en/gallery-transmission-electron-microscopy/Colloidal-Samples/Microcrystalline-Cellulose/index.html

Received 25.02.2024, accepted 25.11.2024